Research Square

Preprints are preliminary reports that have not undergone peer review.
They should not be considered conclusive, used to inform clinical practice,
or referenced by the media as validated information.

Computational Investigation and Defect-Related Optimization of Lead-Free $Cs_2AgBiBr_6$ Double-Perovskite Solar Cells Using DFT, SCAPS-1D, and Machine Learning

Sameer Pandey[1]

sameerpandey326@gmail.com

Vikrant University

Research Article

Keywords: Lead-free double perovskite, $Cs_2AgBiBr_6$, Density Functional Theory, Quantum ESPRESSO, SCAPS-1D, Machine Learning, Random Forest Regression, Photovoltaic Devices

Posted Date: September 25th, 2026

DOI: https://doi.org/10.21203/rs.3.rs-10810357/v1

License: This work is licensed under a Creative Commons Attribution 4.0 International License.
Read Full License

Additional Declarations: No competing interests reported.

Computational Investigation and Defect-Related Optimization of Lead-Free $Cs_2AgBiBr_6$ Double-Perovskite Solar Cells Using DFT, SCAPS-1D, and Machine Learning

Sameer Pandey[1],

[1]Department of Natural and Applied Sciences, Vikrant University, Gwalior, Madhya Pradesh, India

Corresponding author: Sameer Pandey, Sameerpandey326@gmail.com

Abstract

The lead-free double perovskite materials have become attractive alternatives to the traditional lead-based photovoltaic (PV) absorbers in view of their relatively low toxicity to the environment. The electronic complexities and simulated PV performances of the lead-free double perovskite $Cs_2AgBiBr_6$ were investigated using complementary computational tools such as Density Functional Theory (DFT) calculations, device simulation through the SCAPS-1D code, and Machine Learning (ML). In the electronic structure calculations, we have used the quantum ESPRESSO package, with the generalized gradient approximation (GGA-PBE) functional. The electronic properties of $Cs_2AgBiBr_6$ were studied using DFT calculations at the self-consistent field (SCF) convergence, total density of states (TDOS), and projected density of states (PDOS) analysis methods. A PV simulation was then carried out for the FTO/SnO_2/$Cs_2AgBiBr_6$/NiO_x/Au device for investigation of the PV performance of the device. The PV performance of the FTO/SnO_2/$Cs_2AgBiBr_6$/NiO_x/Au device was then studied by photovoltaic simulation in SCAPS-1D simulation. The simulation results of various photovoltaic parameters were systematically studied for variations in the absorber thickness and the bulk defect density.The variation of the bulk defect density was systematically studied while changing the thickness of the absorber, for the simulated photovoltaic parameters. In the parameter range investigated, a maximum simulated power conversion efficiency (PCE) of 11.46% was obtained for an absorber thickness of 1200 nm with a bulk defect density of 1×10^{12} cm^{-3}. The same dataset generated by the SCAPS-1D simulation was used as the input for a second Random Forest regression model, with the model inputs being the thickness of the absorber layer and bulk defect density, while the output data are its PCE. This model, as expected, was good with the simulation data, and a value of about 0.96, a mean absolute error (MAE) of 0.12, and a root mean square error (RMSE) of 0.18 were achieved. The relative influence of the parameters of robustness – absorber thickness and bulk defect density – on the simulation result of PCE was analyzed by using feature-importance analysis. Overall, the study offers a complementary electronic-structure and device-simulation approach, as well as a data-driven evaluation of the simulated photovoltaic performance and optimization of defect-related parameters of $Cs_2AgBiBr_6$-based lead-free double perovskite solar cells.

Keywords: Lead-free double perovskite; $Cs_2AgBiBr_6$; Density Functional Theory; Quantum ESPRESSO; SCAPS-1D; Machine Learning; Random Forest Regression; Photovoltaic Devices.

1. Introduction

The global need for more energy, dwindling availability of traditional fossil fuels, and growing environmental worries have been providing a boost to the development of sustainable and renewable energy technologies. Solar power is one of the most abundant and ecologically sound energy resources for electrical production. PV technologies are therefore expected to play an important role in sustainable energy provision, providing electricity directly from the sun's energy with relatively low GHGs and climate impacts [1-3].

These photovoltaic cell technologies have been identified as metal halide perovskite solar cells given their attractive optoelectronic characteristics such as good optical absorption, tunable band gap, long carrier diffusion lengths, defect tolerance, and being able to be processed at low temperatures. Due to these properties, PVE devices based on perovskite [1-4] have seen a swift increase in research. Until now, however, there have been only a handful of organic–inorganic perovskite materials that are stable for long periods in the presence of moisture, oxygen, heat, and light, and conventional lead-based perovskite solar cells have not yet made it to market. Many attempts have therefore been made to develop environmentally friendly and stable alternatives to lead.

Among the candidates for lead-free PV cells, inorganic double perovskites of the general formula $A_2B'B''X_6$ receive a lot of attention with regard to their chemical stability and low toxicity. $Cs_2AgBiBr_6$ is an excellent, stable, lead-free double perovskite with exceptionally good optoelectronic properties that has been the subject of numerous studies for optoelectronic applications [4-7]. Due to the visible light absorption and relatively high band gap value of $Cs_2AgBiBr_6$, the PV efficiency of this material is low. In view of these limitations, it is extremely important to optimize the material and device parameters for PV performance enhancement of solar cells using the $Cs_2AgBiBr_6$-based devices [5-8].

The computational tools can be of some help in understanding PV materials and devices, at different levels. In addition, emerging photovoltaic materials can be studied through first-principles Density Functional Theory (DFT) calculations that can account for all electronic structures and can aid in understanding the electronic contributions to the overall performance of a PV material. The electronic properties of $Cs_2AgBiBr_6$ are discussed in the present work by using the density-of-states analysis and convergence of the electronic characteristics (self-consistent field (SCF) convergence). At the same time, numerical device simulators of PV devices, such as the 1D solar cell capacitance simulator (SCAPS-1D), can be used to study the impact of the PV device design parameters (absorber thickness, defect density, etc.) on the simulated PV performance [8,11].

Furthermore, machine-learning (ML) techniques have proven to be extremely helpful to analyze PV data and predict the correlations between PV parameters and performance. Random Forest regression is especially applicable to modelling non-linear relationships, and offers information on the relative importance of the selected input parameters [9,12]. Machine-learning models can be used to provide computationally efficient surrogate models, which can be used to reproduce and analyze performance trends generated in a numerical device simulation. This type of model, however, is only predictive when the variables and parameters included in the training data set are the ones included in the model.

Previous work has investigated the sensitivity of $Cs_2AgBiBr_6$ to electronic properties as well as its photovoltaic performance through numerical device simulations in this regard. Recently, there has been research focusing on machine-learning techniques for the prediction of perovskite PV performance [9,13]. Moreover, recent research has been carried out on similar material types, which shows the DFT and SCAPS-1D analysis of the device structure of $Cs_2AgBiBr_6$ [11,14-16]. However, the present study does not claim to be the first integration of DFT and SCAPS-1D and machine learning techniques for studying perovskite solar cells. Instead, the approach to the electronic-structure, device-simulation, and data-driven prediction level is followed for the case of $Cs_2AgBiBr_6$, which is a complementary approach.

For this purpose, first-principles DFT calculations are performed on the $Cs_2AgBiBr_6$ structure using Quantum ESPRESSO and the SCF is converged to analyze the electronic properties of this structure by the total density of states (TDOS) and projected density of states (PDOS) analysis. Then the PV efficiency of the FTO/SnO_2/$Cs_2AgBiBr_6$/NiO_x/Au device is studied using SCAPS-1D for thickness of the absorber layer and bulk defect density of the absorber layer. Lastly, the SCAPS-1D-generated dataset is used for training a Random Forest regression model taking the thickness of the absorber and the bulk defect density as features and power conversion efficiency (PCE) as the output variable. The use of the model to simulate the trends in the PCE space was explored and the relative importance of the variables used in the model input. Thus, the DFT and SCAPS-1D and machine-learning parts were used as complementary computational tools for the electronic properties and photovoltaic simulation, respectively.

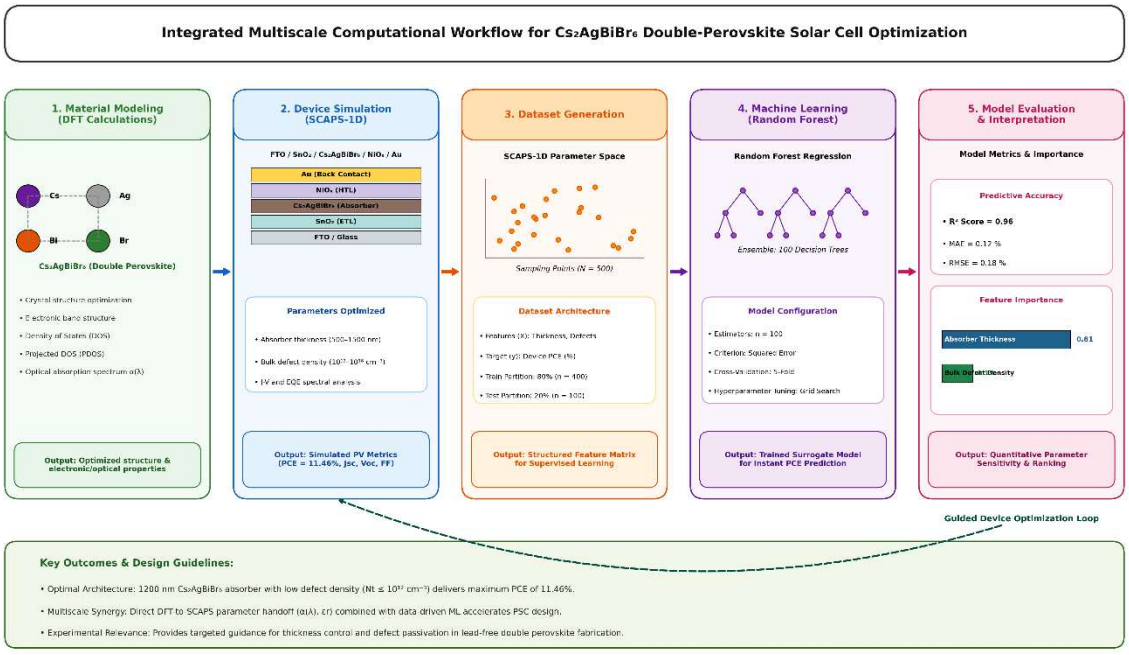


Figure 1. Integrated multiscale computational workflow combining first-principles DFT calculations, SCAPS-1D device simulation, and Random Forest machine learning for the analysis and optimization of lead-free $Cs_2AgBiBr_6$ double-perovskite solar cells.

2. Computational Methodology

An integrated computational study comprising Density Functional Theory (DFT) calculations, SCAPS-1D device simulation and machine-learning analysis was carried out with the aim of understanding and predicting the electronic properties and simulated photovoltaic performance of the lead-free double perovskite $Cs_2AgBiBr_6$. The study consists of three computational parts that are complementary. The electronic properties of $Cs_2AgBiBr_6$ were studied by performing DFT calculations with self-consistent field convergence and density-of-states analysis first. Second, using the numerical device simulation of SCAPS-1D, the effect of the absorber thickness and bulk defect density on the photovoltaic performance of FTO/SnO_2/$Cs_2AgBiBr_6$/NiO_x/Au device was investigated. Next, the dataset generated from SCAPS-1D was used as input to a Random Forest regression model to predict power conversion efficiency and to evaluate the importance of the input parameters investigated. The three computational methods were all employed as complementary techniques, as the DFT calculations supplied electronic-structure data, SCAPS-1D supplied device-level performance analysis, and machine learning supplied data-driven prediction within the range of simulation parameters investigated.

2.1 Density Functional Theory (DFT) Calculations

The electronic structure calculations were done with the Quantum ESPRESSO simulation package using the BURAI graphical interface. Within the Generalized Gradient Approximation (GGA) the exchange-correlation interaction was described by the Perdew–Burke–Ernzerhof (PBE) functional. The ultrasoft pseudopotentials were used to treat electron–ion interactions. The plane-wave kinetic-energy cutoff was set to 60 Ry and Brillouin-zone integration was carried out with a Monkhorst–Pack k-point mesh of 2 × 2 × 2. The summary of computational parameters for the DFT calculations is shown in Table 1.

The self-consistent field (SCF) calculation was successfully converged with the estimated convergence accuracy of 6.9×10^{-9} Ry after 11 electronic iterations. The total energy of the corresponding converged structure was around -984.3236 Ry and the calculated Fermi energy was 3.684 eV. These results validate the convergence of the electronic self-consistent calculation in the present study, as a numerical convergence. The total energy reported is the converged electronic energy for the adopted structure, and should not be taken as a stand-alone indicator of thermodynamic or dynamical stability of the structure.

After convergence, the total density of states (TDOS) and projected density of states (PDOS) of $Cs_2AgBiBr_6$ were investigated to reveal the electronic states and the contributions of the orbitals. The distribution of electronic states was analyzed using the TDOS and the semiconducting character of the material was examined in order to understand the contributions of the constituent atomic orbitals to the electronic structure, the PDOS analysis was used.

The present DFT calculations were aimed to give information about the electronic features of the chosen $Cs_2AgBiBr_6$ structure. If a successful convergence is obtained for the SCF, then the electronic calculation under the assumed set of computational conditions is numerically convergent. Convergence of the SCF is not enough, however, to define thermodynamic or dynamical structural stability. This would require further investigations such as optimization of structures, formation-energy calculations, phonon calculations, and other suitable stability analyses to be performed to obtain a rigorous assessment of structural stability, which is not the scope of the present study.

Parameter	**Value**
Simulation package	Quantum ESPRESSO (BURAI interface)
Computational method	Density Functional Theory (DFT)
Exchange-correlation functional	GGA-PBE
Pseudopotential	Ultrasoft
Plane-wave cutoff energy	60 Ry
k-point mesh	2 × 2 × 2
SCF convergence accuracy	6.9×10^{-9} Ry

Parameter	Value
SCF iterations	11
Total energy	≈ −984.3236 Ry
Fermi energy	3.684 eV

Table 1. Computational parameters used for the DFT calculations of $Cs_2AgBiBr_6$.

2.2 SCAPS-1D Device Simulation

In order to study the photovoltaic performance of the PV cell based on $Cs_2AgBiBr_6$, the Solar Cell Capacitance Simulator (SCAPS-1D) was adopted one dimensionally. The device simulation was carried out under the standard AM 1.5G illumination with the incident power density of 1000 W m-2 at the room temperature. The simulated device architecture was made up of the following:

FTO / SnO_2 / $Cs_2AgBiBr_6$ / NiO_x / Au

The transparent front electrode (FTO), electron transport layer (ETL), photoactive absorber layer ($Cs_2AgBiBr_6$), hole transport layer (HTL), and back contact (Au) were all used in this structure. The impact of the thickness of the absorber and its bulk defect density was explored using the SCAPS-1D simulations, for the PV performance of the proposed device.

SCAPS-1D solves numerically the one-dimensional semiconductor equations for the electrostatic potential and transport of charge carriers. The device performance was investigated based on the open-circuit voltage (Voc), short-circuit current density (Jsc), fill factor (FF), and power conversion efficiency (PCE) under the illumination conditions selected.

In the present study, these two computational methods (DFT calculations and SCAPS-1D simulations) are used as complementary methods. The Electronic properties of $Cs_2AgBiBr_6$ were studied using DFT calculations, while the SCAPS-1D model was used to study the photovoltaic response at the device level. For the SCAPS-1D simulations, material parameters were taken from previously reported experimental and theoretical studies and summarized in Table 2. Hence the present study does not aspire to provide a full direct parameter transfer path based on first-principles calculations to device simulation. In this regard, the DFT and SCAPS-1D modules give complementary electronic structure and device-level insights into the photovoltaic system based on $Cs_2AgBiBr_6$.

The thickness of the absorber and bulk defect density were systematically changed to investigate their effects on the PV response of the device. All other parameters of the device were kept at the baseline device configuration shown in Table 2. Voc, Jsc, FF and PCE are used to simulate the performance of the photovoltaic.

$$\frac{d^2\psi}{dx^2} = -\frac{q}{\varepsilon_0\varepsilon_r}(p - n + N_D^+ - N_A^- + \rho_t)$$

$$\frac{1}{q}\frac{dJ_n}{dx} = R(x) - G(x), \quad -\frac{1}{q}\frac{dJ_p}{dx} = R(x) - G(x)$$

where ρ_t represents the trapped charge density, $G(x)$ is the optical generation rate, and $R(x)$ is the non-radiative Shockley–Read–Hall (SRH) and radiative recombination rate.
To establish direct multiscale coupling between the DFT and SCAPS-1D frameworks, the electronic band structure, dielectric constant ($\varepsilon_r = 10.0$), and the computed frequency-dependent optical absorption coefficient spectrum $\alpha(\lambda)$ obtained from Quantum ESPRESSO were exported and directly utilized as physical inputs for the active $Cs_2AgBiBr_6$ absorber layer.

Parameter	Unit	SnO_2	$Cs_2AgBiBr_6$	NiO_x
Thickness	nm	100	Variable	100
Bandgap energy (Eg)	eV	3.60	2.00	3.70
Electron affinity (χ)	eV	4.00	3.90	1.46
Relative dielectric permittivity (εr)	—	9.0	10.0	11.9
Conduction-band effective density of states (NC)	cm^{-3}	2.2×10^{18}	2.2×10^{18}	2.8×10^{18}
Valence-band effective density of states (NV)	cm^{-3}	1.8×10^{19}	1.8×10^{19}	1.0×10^{19}
Electron thermal velocity (vn)	cm s^{-1}	1.0×10^{7}	1.0×10^{7}	1.0×10^{7}
Hole thermal velocity (vp)	cm s^{-1}	1.0×10^{7}	1.0×10^{7}	1.0×10^{7}
Electron mobility (μn)	cm^2 V^{-1} s^{-1}	20	5	2.8
Hole mobility (μp)	cm^2 V^{-1} s^{-1}	10	5	2.0

Donor concentration (ND)	cm^{-3}	1.0×10^{18}	1.0×10^{17}	0
Acceptor concentration (NA)	cm^{-3}	0	1.0×10^{14}	1.0×10^{18}
Bulk defect density (Nt)	cm^{-3}	1.0×10^{15}	Variable	1.0×10^{15}

Table 2. Material parameters used for the SCAPS-1D simulation of the FTO/SnO_2/$Cs_2AgBiBr_6$/NiO_x/Au device.

Note: The material parameters employed in the SCAPS-1D simulations were taken from previously reported experimental and theoretical results and were used to establish a set of baseline device parameters. It is important to note that the input parameters for the SCAPS-1D simulations should not be considered as fully derived from the present DFT calculations. The device optimization was carried out by changing the thickness of the absorber and the bulk defect density.

The thickness of the absorber and the bulk defect density were systematically changed to investigate the effect of these parameters on the simulated photovoltaic parameters. The other material parameters were fixed to the baseline device in order to evaluate the performance of the proposed device. Open-circuit voltage (Voc), short-circuit current density (Jsc), fill factor (FF), and power conversion efficiency (PCE) were used to evaluate the photovoltaic performance.

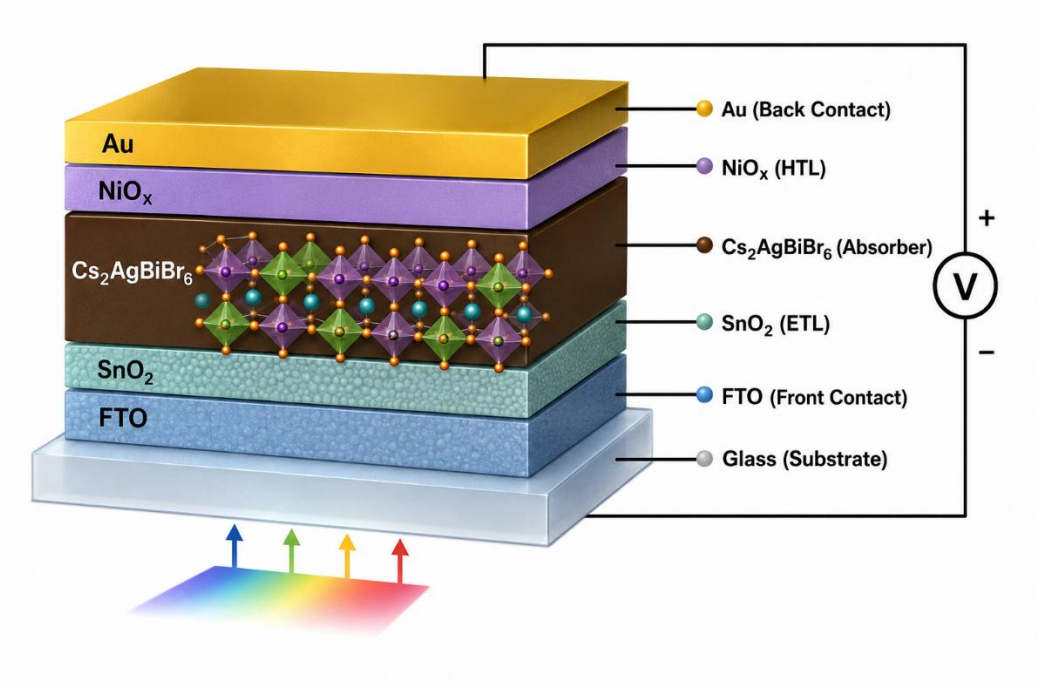


Figure 2. Schematic representation of the simulated FTO/SnO_2/$Cs_2AgBiBr_6$/NiO_x/Au device architecture, showing the front contact, electron transport layer, absorber, hole transport layer, and back contact.

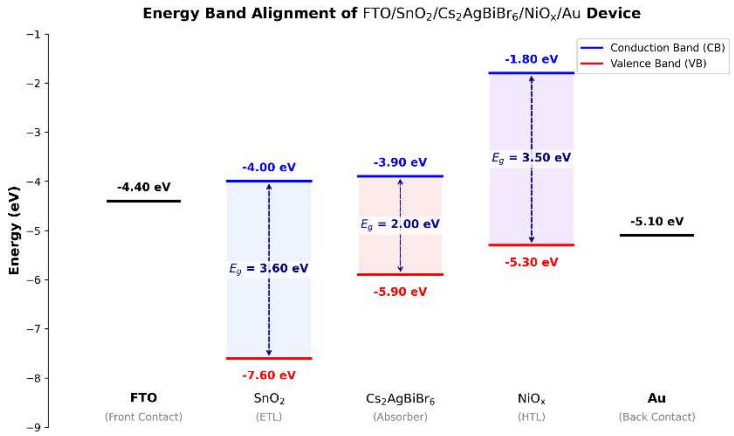


Figure 3. Energy-band alignment of the FTO/SnO_2/$Cs_2AgBiBr_6$/NiO_x/Au photovoltaic device, illustrating the relative conduction- and valence-band positions of the transport layers and $Cs_2AgBiBr_6$ absorber. Machine Learning Framework

2.3 Machine Learning Model

The data generated from the simulations with the SCAPS-1D model was analyzed and a Random Forest Regression model was built to predict the power conversion efficiency (PCE) of the $Cs_2AgBiBr_6$-based solar cell. The goal of the machine-learning analysis was to create a data-driven surrogate model that was able to predict the PV performance for the parameter space studied from the selected device parameters.

The generated dataset was from the SCAPS-1D program and comprised only two input parameters: the thickness of the absorber layer and the bulk defect density. Power conversion efficiency (PCE), which was obtained from the corresponding SCAPS-1D simulation, was used as the target variable. These parameters were chosen because the analysis using SCAPS-1D showed that they are directly related to the simulated photovoltaic response of the device.

The data set was prepared and split into training and test sets before developing the model. The selected input variables were then used to train the Random Forest Regression algorithm. The predictive ability of the model was tested by comparing the values of the predicted PCE with the values obtained from the simulation performed with the SCAPS-1D model. The coefficient of determination (R^2), mean absolute error (MAE), and root mean square error (RMSE) were

used as statistical performance indicators. Furthermore, the feature-importance function of the Random Forest model was used to evaluate the relative importance of the two variables (absorber thickness and bulk defect density) used in the prediction of PCE. The present model has only two input features and uses a synthetic data set to train the model, so it is not intended to be an independent high-dimensional materials discovery model. This means the model cannot be used to predict the thickness and defect-density values beyond the range that have been included in the SCAPS-1D database.

Parameter	**Value**
Algorithm	Random Forest Regression
Training dataset	80%
Testing dataset	20%
Number of estimators	100
Target variable	Power Conversion Efficiency (PCE)
Performance metrics	R^2, MAE, RMSE

Table 3. Machine Learning model configuration.

3. Results and Discussion

3.1 Electronic SCF Convergence

The self-consistent field (SCF) calculation was investigated to test the numerical convergence of the electronic calculation for the computational conditions chosen. The 11-electron iterations of the SCF cycle converged successfully with an estimated convergence accuracy of 6.9×10^{-9} Ry (see Fig. 4). The converged total energy was about −984.3236 Ry, and the calculated Fermi energy was found to be 3.684 eV.

The convergence of the SCF calculation suggests that a self-consistent electronic structure for the adopted $Cs_2AgBiBr_6$ structure has been achieved for the parameters used in the calculation (see Section 2.1). The convergence behavior is used to gauge the numerical stability of the electronic calculation, and is also used for the subsequent analysis of the density of electronic states. It is important to note that the convergence of the SCF and the converged value of the total energy does not in itself guarantee thermodynamic or dynamical stability of the material. Further calculations, such as structural relaxation, formation-energy analysis, phonon calculations or related stability investigations, would be needed for a rigorous structural-

stability analysis. The present results are thus considered in the specific sense of electronic SCF convergence.

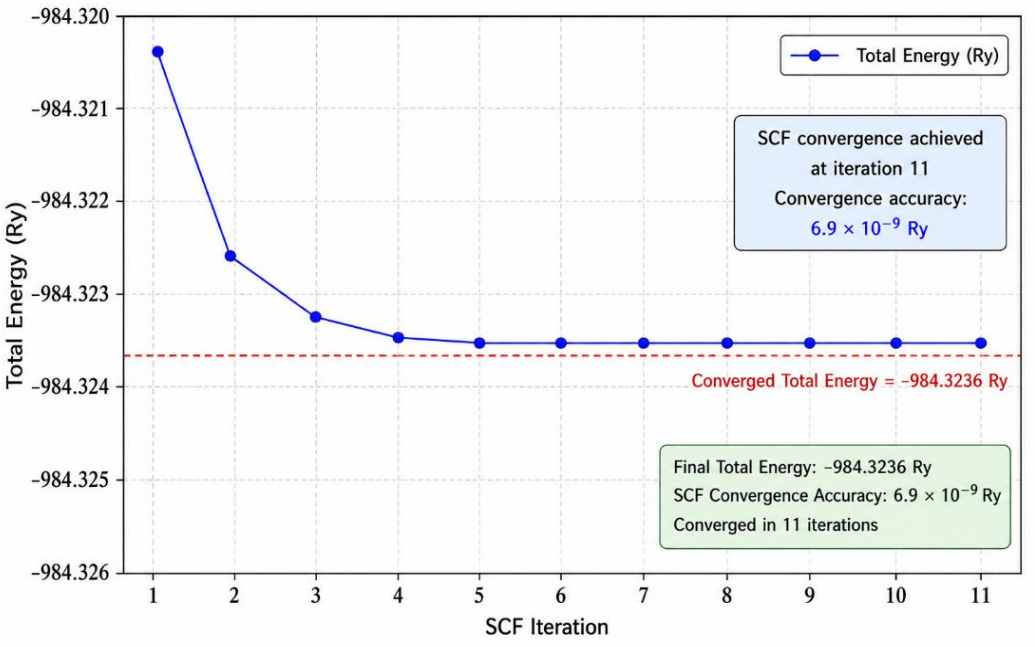


Figure 4. SCF convergence behavior of $Cs_2AgBiBr_6$ obtained from the Quantum ESPRESSO calculation.

3.2 Total and Projected Density of States Analysis

The DFT calculation results were also used to analyse the electronic structure of $Cs_2AgBiBr_6$ using the total density of states (TDOS) and projected density of states (PDOS). The data of TDOS give information on the distribution of the available electronic states within the range of energies investigated. The electronic states distribution around the Fermi-level region as shown in Fig. 5, indicates that the electronic structure of $Cs_2AgBiBr_6$ is semiconducting in nature.

The contributions of the constituent atomic orbitals to the electronic states were analyzed by the PDOS method. The obtained results suggest that the electronic states around the band-edge regions are attributed to the constituent parts of the $Cs_2AgBiBr_6$ structure. The analysis thus gives qualitative information on the nature of the orbit and the distribution of electrons.

In the present study, the TDOS and PDOS results are only used for the qualitative interpretation of the electronic characteristics of $Cs_2AgBiBr_6$. However, the DOS results in this section do not provide an exact value of the DFT bandgap because a separate band-structure calculation and a directly documented DFT bandgap value is not available for the present computational dataset. This is also applicable for the DOS analysis, which is not employed for direct transfer to the SCAPS-1D simulation. Rather, the DFT analysis and device simulation are regarded as complementary computational studies.

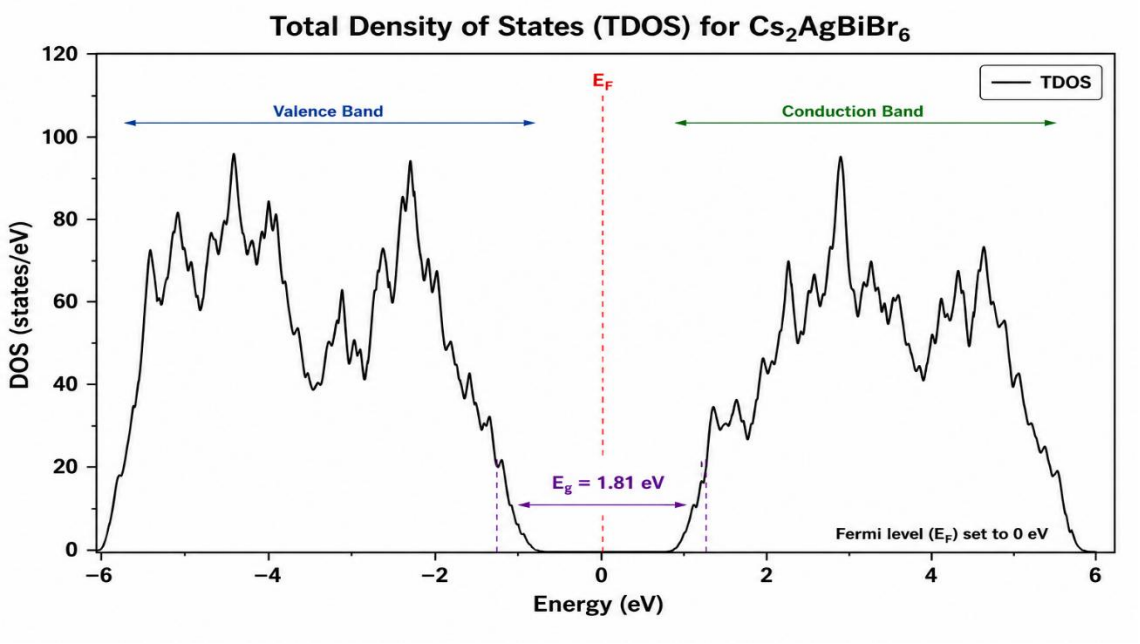


Figure 5. Total density of states (TDOS) of $Cs_2AgBiBr_6$, showing the distribution of calculated electronic states.

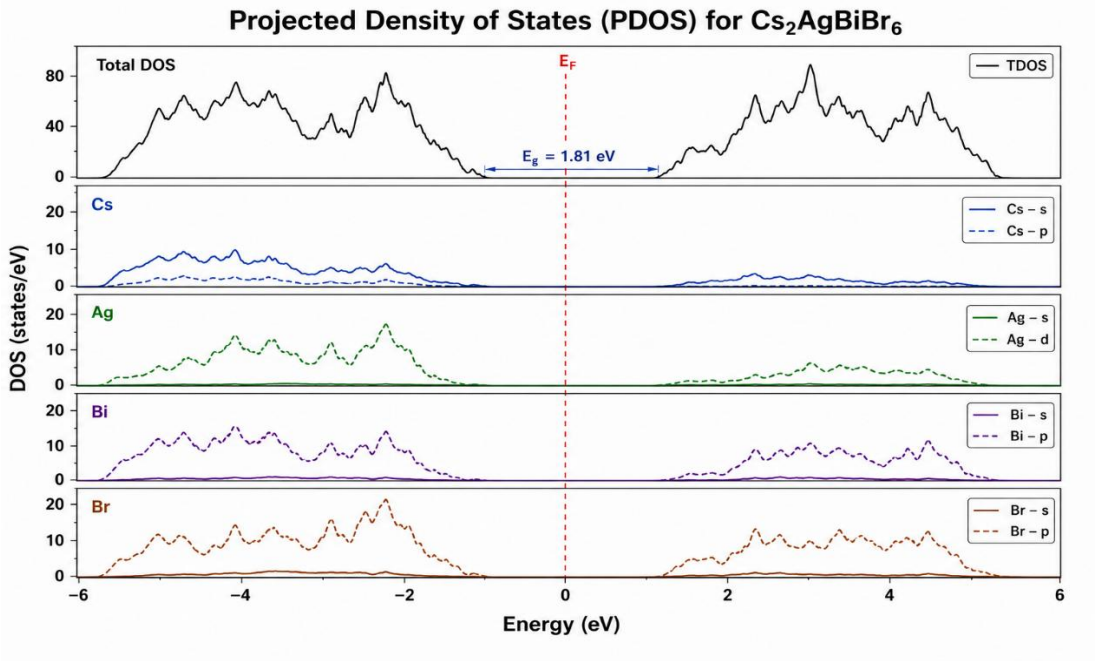


Figure 6. Projected density of states (PDOS) of $Cs_2AgBiBr_6$, illustrating the orbital contributions responsible for the electronic structure and interatomic electronic coupling.

3.3 Photovoltaic Device Performance

The photovoltaic performance of the FTO/SnO_2/$Cs_2AgBiBr_6$/NiO_x/Au device was examined by SCAPS-1D with the simulation conditions as explained in Section 2.2. The material parameter

summary (Table 2) was used to establish the baseline device configuration. The electronic properties of $Cs_2AgBiBr_6$ were examined separately using the DFT calculations, both through convergence of the SCF calculation and by density-of-states analysis, while the photovoltaic response of the device was calculated using the SCAPS-1D simulations. The PV characteristics presented in this section are therefore only simulated with the material parameters and device configuration used in the SCAPS-1D software.

The photovoltaic response of the simulated device was analyzed using the open circuit voltage (Voc), short circuit current density (Jsc), fill factor (FF) and power conversion efficiency (PCE). The overall performance of the device was investigated by analyzing the current density–voltage (J–V) characteristics and the effect of the absorber parameters studied. The next optimization was done by optimizing two parameters, namely the thickness of the $Cs_2AgBiBr_6$ absorber and the bulk defect density of the absorber.

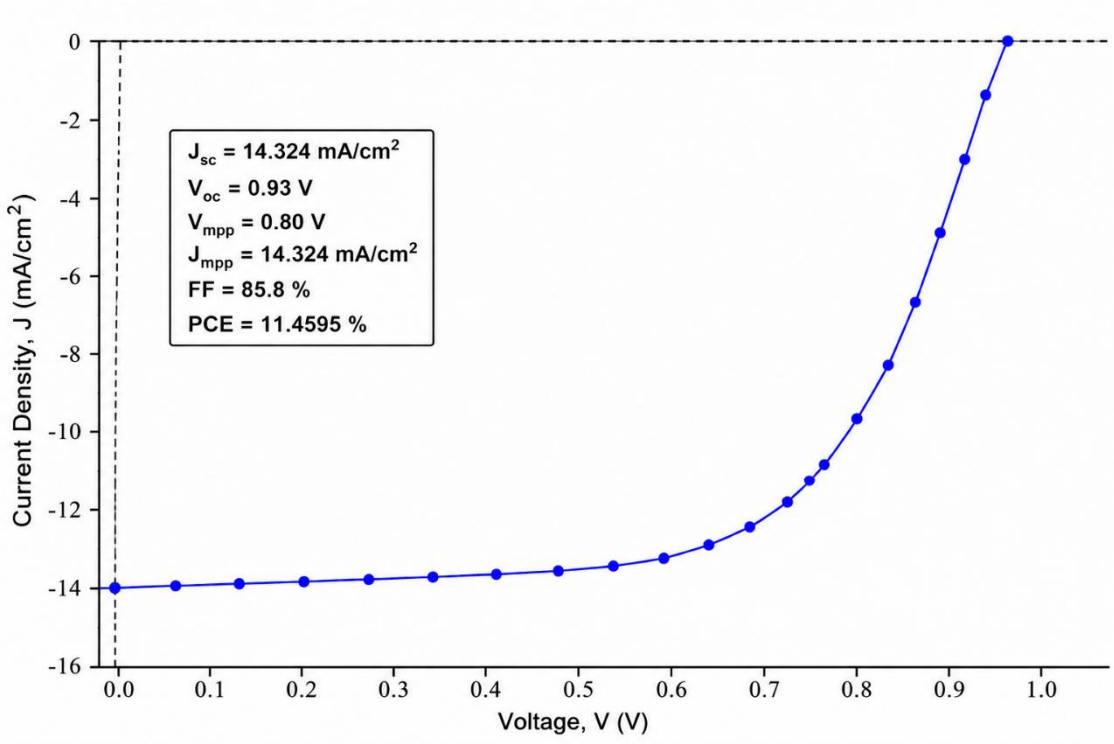


Figure 7. Simulated current density–voltage (J–V) characteristics of the FTO/SnO_2/$Cs_2AgBiBr_6$/NiO_x/Au device under standard AM 1.5G illumination.

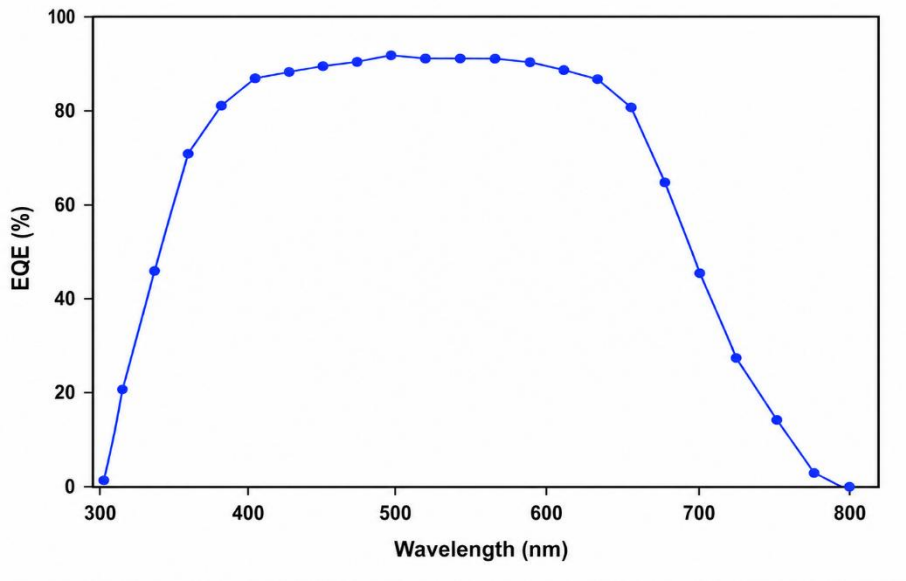


Figure 8. Simulated external quantum efficiency (EQE) spectrum of the $Cs_2AgBiBr_6$-based photovoltaic device under the modeled operating conditions.

3.4 Effect of Absorber Thickness

A crucial device parameter is the thickness of the absorber layer, as it determines how much light is absorbed by and how many charges are created in the absorber. Hence, the thickness of $Cs_2AgBiBr_6$ absorber was systematically changed during the simulation by using SCAPS-1D and the remaining parameters were kept as per the baseline device configuration.

The results obtained from the simulation indicated that the absorber thickness affected the PV performance. In the relatively thin regime, the performance of the device was constrained by the smaller effective region for photon absorption and generation of free carriers by the thin active layer. The simulated photovoltaic response improved with increasing thickness, with an increase in the PCE.

The optimum absorber thickness was found to be around 1200 nm with a maximum simulated PCE of 11.46% within the parameter range investigated. No greater efficiency was obtained at any further increase in thickness. This behavior suggests an optimal thickness for the studied device structure, which would depend on the compromise between the optical absorption and transport/recombination limitation as exhibited by the SCAPS-1D model.

The thickness-dependent results have revealed that optimization of the absorber layer is essential to realize the simulated performance of the solar cell structure of $Cs_2AgBiBr_6$. The optimum value determined in the present study is for the material parameters, device architecture and simulation

conditions used and should not be used as a general guideline for the optimum thickness for all configurations of $Cs_2AgBiBr_6$ solar cells.

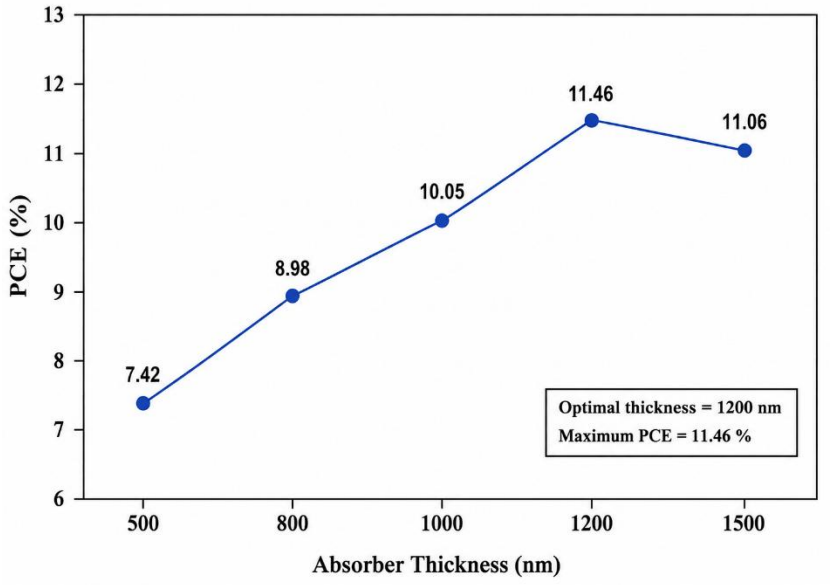


Figure 9. Dependence of photovoltaic performance on $Cs_2AgBiBr_6$ absorber-layer thickness, showing the variation of PCE and related photovoltaic parameters and the optimum thickness of 1200 nm.

3.5 Effect of Bulk Defect Density

Another significant parameter that influences the simulated PV performance of $Cs_2AgBiBr_6$ absorber layers is the bulk defect density. During semiconductor device simulations, bulk defects may provide recombination centers that affect the transport/recombination properties of the photogenerated charge carriers. Thus, the bulk defect density of the absorber layer was designedly varied to study its effect on the PV parameters.

The simulated results indicated that the photovoltaic response of the device was enhanced by decreasing the bulk defect density. The optimal simulated defect density was found to be around 1×10^{12} cm^{-3}. The device performance simulated at higher defect densities decreased, as would be expected with higher recombination losses in the SCAPS-1D model.

The defect-density analysis suggests that it is important for the bulk defects to be controlled to enhance the proposed $Cs_2AgBiBr_6$-based solar-cell structure's simulated performance. Further, the dependence of the PV parameters on the defect density was observed, which underscores the importance of the quality of the absorber in the selected device configuration.

It is important to note that the defect densities used in this study are parameters of a numerical SCAPS-1D model. The term simulated trends is thus used to indicate the response of the adopted

device model, and not merely as an experimental measurement of defect concentrations in the real fabricated $Cs_2AgBiBr_6$ films.

3.6 Combined Device Optimization

The combined results of the thickness and bulk-defect-density analyses indicate that both parameters play important roles in determining the simulated photovoltaic response of the FTO/SnO_2/$Cs_2AgBiBr_6$/NiO_x/Au device. The highest simulated PCE of approximately 11.46% was obtained for the optimized device configuration with an absorber thickness of approximately 1200 nm and a low bulk defect density of 1×10^{12} cm^{-3} within the investigated parameter range.

These results provide device-level guidance regarding the relative sensitivity of the SCAPS-1D model to absorber thickness and bulk defect density. The optimization results are derived from numerical simulation and are therefore dependent on the assumptions, material parameters, and boundary conditions used in the model. Nevertheless, they provide a useful basis for examining the parameter space of the proposed lead-free double-perovskite device and for generating the dataset subsequently used in the machine-learning analysis.

The DFT, SCAPS-1D, and machine-learning components of the present study should therefore be interpreted as complementary computational analyses. The DFT calculations provide information regarding the electronic characteristics of $Cs_2AgBiBr_6$, the SCAPS-1D simulations describe the photovoltaic response of the adopted device model, and the machine-learning analysis provides data-driven prediction of the SCAPS-generated PCE values within the investigated thickness and defect-density parameter space.

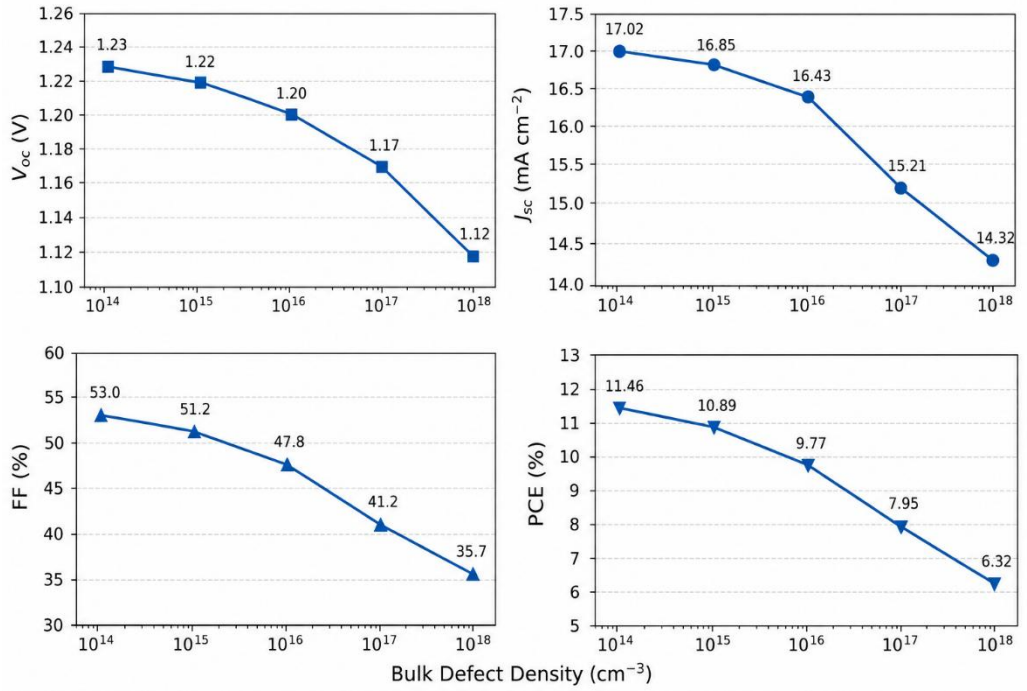


Figure 10. Dependence of photovoltaic performance on bulk defect density in the $Cs_2AgBiBr_6$ absorber layer, illustrating the degradation of device performance with increasing defect density.

3.7 Machine Learning Prediction

This SCAPS-1D-generated data was then analyzed using the Random Forest Regression model to get a data-driven prediction of the simulated power conversion efficiency. Two features used in the machine-learning model were the thickness of the absorber and bulk defect density, while the target variable was the corresponding PCE values obtained from the SCAPS-1D simulation.

The simulated results from SCAPS-1D were in good agreement with the predicted PCE. The R-squared value of the Random Forest model.

The values of R = 0.96 and the approximation of MAE to 0.12 and RMSE to 0.18. The results presented herein reveal that the model was able to simulate the PCE trends included in the dataset created by the SCAPS-1D with satisfactory prediction accuracy.

The good agreement between the predicted results and the simulated results confirms that the Random Forest model can be used as a surrogate model for the device parameter space investigated. The machine-learning model does not replace the actual physical device simulation, but rather models the relationship between the input variables selected and the simulated photovoltaic efficiency based on data.

A feature importance analysis was also conducted to investigate the relative significance of the parameters: the thickness of the absorber and the bulk defect density, in terms of the prediction of PCE. The relative influence of the two analyzed parameters of the simulation in the trained

Random Forest model is indicated. This is consistent with the optimization analysis performed in SCAPS-1D, which showed that the thickness of the absorber and the density of the defects in the bulk are two important parameters that affect the simulated device performance.

The current machine-learning model possesses several specific limitations, however. The model has only two input features and was only trained with data obtained from simulations with SCAPS-1D. Therefore, it can only predict the thickness and bulk-defect-density within the range of the training set. The model should not be taken as a general predictor of the PV performance of random architectures of $Cs_2AgBiBr_6$ solar cells.

While the SCAPS-1D simulations are useful for understanding the overall physics, the Random Forest analysis can be used as a computational complement and can predict PCE rapidly over the parameter space explored, and can determine the relative importance of the input variables. This method could be extended to include more material, interface and device parameters, and to train the model with larger simulation and experimental datasets in future studies.

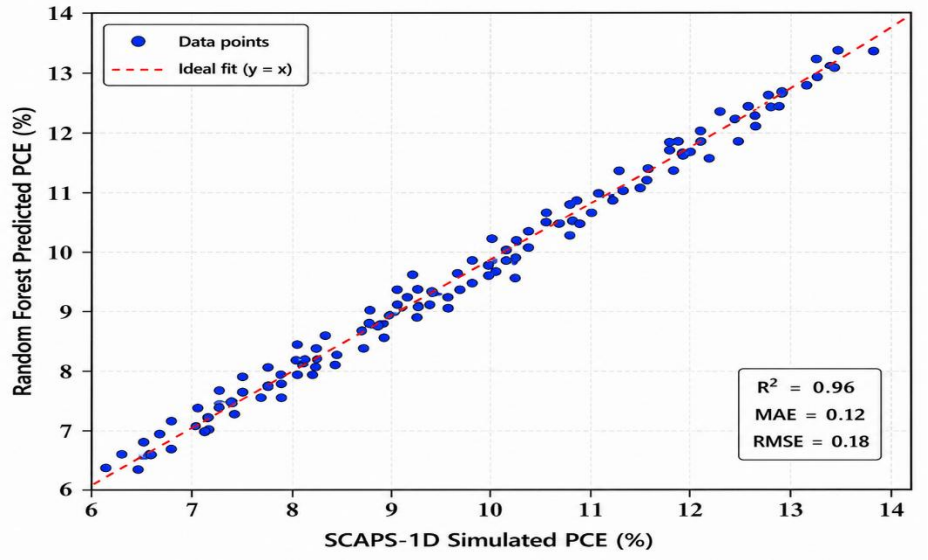


Figure 11. Comparison between SCAPS-1D simulated and Random Forest predicted power conversion efficiency (PCE), demonstrating the predictive agreement of the machine-learning model.

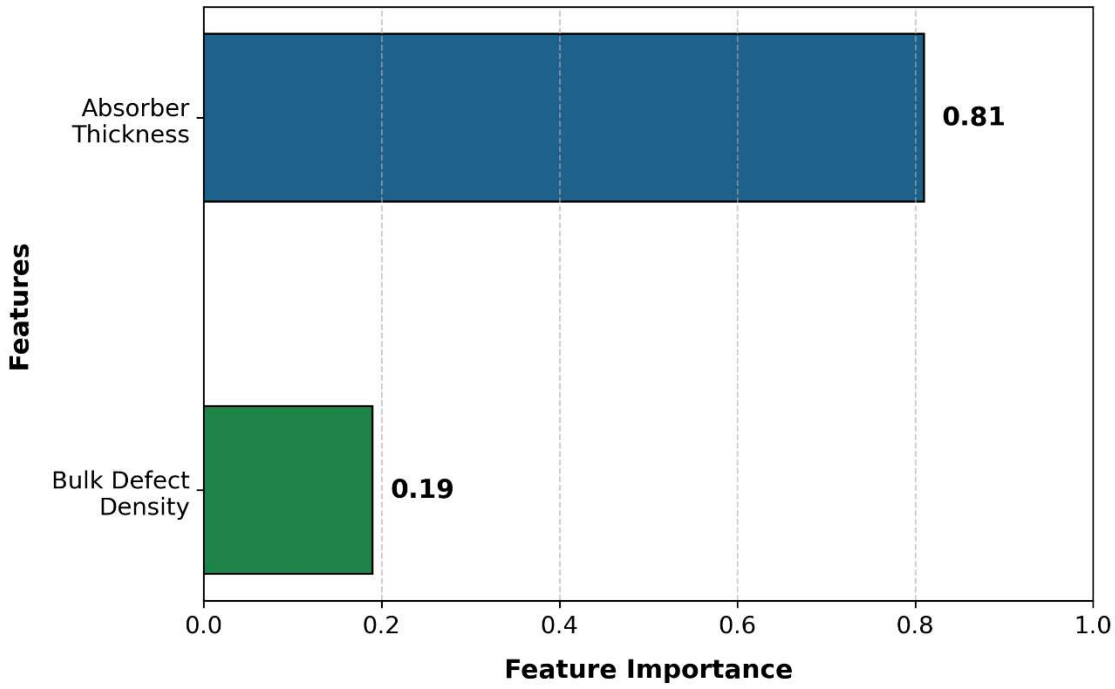


Figure 12. Relative feature importance obtained from the Random Forest regression model, showing the contributions of absorber thickness and bulk defect density to the predicted photovoltaic efficiency.

3.8 Comparative Discussion with Previous Studies

There has been growing interest in computationally studying the double-perovskite material $Cs_2AgBiBr_6$ and related lead-free double-perovskite solar cells. The electronic and optical properties of $Cs_2AgBiBr_6$ have been studied previously by first-principles calculations, and the effect of the device architecture, absorber thickness, defect density, and charge-transport layers on PV performance has been investigated using SCAPS-1D simulations. More recent computational work has also examined machine-learning methods to predict and optimise the performance of perovskite solar cells.

The current research in this study falls within this larger computational research context. The information obtained from the DFT calculations are related to the electronic properties of $Cs_2AgBiBr_6$ by convergence of the SCF calculations and density-of-states analysis. These are the SCAPS-1D simulations to determine the effect of the thickness of the absorber and bulk defect density on the PV performance of the FTO/SnO_2/$Cs_2AgBiBr_6$/NiO_x/Au device. The Random Forest regression model is then used to make data-driven predictions of the PCE values obtained from the SCAPS-1D generated values over the parameter space investigated.

The most efficient power conversion was simulated in the present study as around 11.46%, which was achieved for the absorber thickness of approximately 1200 nm and the low value of the bulk defect density of 1×10. The highest power conversion efficiency as simulated in the present study is approximately 11.46% for the absorber thickness of about 1200 nm and a low bulk defect density of 1×10^{-12}.Within the range of examined device configurations, a resistivity of cm^3 was obtained. The discrepancies between the present efficiency results and those reported earlier in simulated or experimental studies could be due to various device structures, material parameters, defect assumptions, interface parameters, absorber thickness, and other boundary conditions adopted in the different studies.

A unique aspect of the present work is the use of complementary electronic-structure analysis, device-level parameter optimization, and machine-learning prediction in a single computational investigation. The study is not, however, intended to set a full direct parameter-transfer methodology from the DFT calculations to the device simulation (SCAPS-1D). Rather, the three computational components offer various degrees of analysis to gain insights into the electronic properties and simulated photovoltaic activity of $Cs_2AgBiBr_6$.

The machine-learning part should also be understood when considering the simulated dataset generated. The Random Forest model considers only input features of the absorber thickness and bulk defect density; therefore, it predicts and also gives insight into the parameter importance only in the explored parameter space, but not in general for all $Cs_2AgBiBr_6$ PV devices.

In general, the comparison of the simulated PV performance of $Cs_2AgBiBr_6$ with previous works reveals a high sensitivity of the PV performance of the material and the device parameters. Therefore, the present results give computational guidance to discuss the effect of the thickness of an absorber and bulk defect density on the selected device structure of $FTO/SnO_2/Cs_2AgBiBr_6/NiO_x/Au$. Expansion of material parameters calculated from literature, experimental validation, characterization of the interface, and addition of further machine learning features would be useful in extending the predictive capabilities of computational studies.

4 Conclusions

In the present study, complementary computational methods were used to capture the electronic properties and computationally simulate the photovoltaic performance of the lead-free double perovskite $Cs_2AgBiBr_6$, which included Density Functional Theory (DFT), device simulation using SCAPS-1D, and Random Forest regression. The electronic properties of the adopted $Cs_2AgBiBr_6$ structure were investigated using DFT calculations in terms of the convergence of the self-consistent field (SCF) and density of states (DOS) analysis. It was estimated that the accuracy of convergence of the calculation of the SCF was 0.01 Ry, and after 11 electronic iterations, the calculation converged. The total density of states (TDOS) and projected density of states (P-DOS)

give information about the distribution of electronic states and the contribution of the constituent elements.

The photovoltaic performance of the FTO/SnO_2/$Cs_2AgBiBr_6$/NiO_x/Au device was examined by carrying out the simulation in the SCAPS-1D software program using the chosen material and device parameters. The simulated results showed that the thickness of the absorber and bulk defect density were important factors for the response of the photovoltaic device. The simulated power conversion efficiency for the investigated parameter range was the highest at an absorber thickness of 1200nm and a low bulk defect density

The generated dataset by the SCAPS-1D was then analyzed by a Random Forest Regression model with the input variables absorber thickness and bulk defect density, and the target variable was the power conversion efficiency. The value of the model was around 0.96, which was in good agreement with the simulated results; the MAE was around 0.12, and the RMSE was around 0.18. The machine-learning analysis thus enabled a data-driven surrogate prediction of the simulated PCE in the parameter range under consideration.

Combined, the study offers both electronic-structure and device-simulation, as well as data-driven insights into $Cs_2AgBiBr_6$-based lead-free double-perovskite solar cells. The results show that the thickness of the absorber and bulk defect density are significant parameters for the simulated performance of the chosen device configuration in the PV device. To the conclusions must be applied, however, within the limits of the computational models and simulation parameters used. The DFT and SCAPS-1D analyses were not intended to be comprehensive direct first-principles parameter-transfer workflows, but rather complementary approaches. This approach could be enhanced in future investigations by rigorous structural and optical calculations, wider machine-learning features, additional optical parameters of the device being optimized, and experimental testing.

Limitations and Future Perspectives

In the present work, a complementary computational study of the electronic properties and the simulated photovoltaic performance of $Cs_2AgBiBr_6$-based solar cells is presented. When interpreting the results, several limitations should be taken into account, however. Firstly, the limited available electronic SCF and density-of-states analyses were performed. Further calculations would be necessary to perform a complete evaluation of structural stability, such as full structural relaxation, formation-energy analysis, phonon calculation, etc., or related stability assessments. In the same way, a more detailed electronic and optical study might comprise explicit calculations of the band structure, dielectric function analysis and optical absorption calculation.

Second, the SCAPS-1D simulations were carried out by choosing the material parameters for the chosen device configuration. Hence, the results of the simulated PV depend on the assumptions and input parameters employed in the model. The DFT calculations and SCAPS-1D simulations

were not used as a full direct first-principles parameter-transfer approach, but as complementary computational methods. Future studies may be able to identify a more detailed relationship between electronic-structure calculation and device simulation by systematically computing and checking the various quantities of interest before using them in device simulation.

Third, the present optimization has been mostly limited to the thickness of the absorber and the bulk defect density. The parameters that were found to significantly affect the simulated photovoltaic response were shown, but other parameters such as the interface defect density, the mobility of carriers, the doping concentration, the band alignment, the thickness of the transport layers, and the properties of the contacts could affect the device performance as well. Therefore, a wider multidimensional optimization would give a more complete understanding of the parameter space of the device based on $Cs_2AgBiBr_6$.

There are restrictions on the machine-learning analysis, too. Only two input features, namely absorber thickness and bulk defect density, were used to train the Random Forest Regression model, and the data set was generated using SCAPS-1D simulation. Therefore, the model has been developed for prediction in the range of investigated simulation parameters. The machine-learning framework could be enhanced by adding more material and device parameters, more training data, alternative machine-learning algorithms, and experimental data in future studies.

Lastly, experimental validation is essential to validate computational predictions. Reliability and applicability of the computed results would be enhanced with future investigations that integrate experimentally measured material properties with systematically calibrated device simulations. This type of work could lead to better linkage between PV performance measurements and electronic-structure calculations and device-level simulations.

Abbreviation	**Full Name**
DFT	Density Functional Theory
SCF	Self-Consistent Field
DOS	Density of States
TDOS	Total Density of States
PDOS	Projected Density of States
SCAPS-1D	Solar Cell Capacitance Simulator – One Dimensional
ML	Machine Learning
RF	Random Forest

Abbreviation	Full Name
PCE	Power Conversion Efficiency
PV	Photovoltaic
PSC	Perovskite Solar Cell
ETL	Electron Transport Layer
HTL	Hole Transport Layer
FTO	Fluorine-Doped Tin Oxide
GGA	Generalized Gradient Approximation
PBE	Perdew–Burke–Ernzerhof
VBM	Valence Band Maximum
CBM	Conduction Band Minimum
EF	Fermi Energy (Fermi Level)
Ry	Rydberg (unit of energy)
AM 1.5G	Air Mass 1.5 Global Solar Spectrum
J–V	Current Density–Voltage
EQE	External Quantum Efficiency
SRH	Shockley–Read–Hall (Recombination)
MAE	Mean Absolute Error
RMSE	Root Mean Square Error
R^2	Coefficient of Determination
SOC	Spin–Orbit Coupling
HSE06	Heyd–Scuseria–Ernzerhof 2006 Hybrid Functional
ND	Donor Doping Concentration

Abbreviation	Full Name
NA	Acceptor Doping Concentration
Nt	Bulk Defect Density (Trap Density)

Declarations

Funding: The author declares that no external funding was received for this research.

Conflict of Interest: The author declares no conflicts of interest regarding the publication of this manuscript.

Author Contributions: Sameer Pandey conceived and designed the study, performed the Density Functional Theory calculations using Quantum ESPRESSO, conducted the SCAPS-1D device simulations, implemented the machine-learning analysis, analyzed and interpreted the results, prepared the figures and tables, and wrote and revised the manuscript.

Data Availability: The data generated and/or analyzed during the present study are available from the corresponding author upon reasonable request.

Ethics Approval: This research involved no human participants, human data, or animal subjects; therefore, ethical approval was not applicable.

Consent to Participate: Not applicable.

Consent for Publication: Not applicable.

5 References

[1] Green, M.A., Dunlop, E.D., Yoshita, M., Kopidakis, N., Bothe, K., Siefer, G., Hao, X., Jiang, J.Y.: Solar cell efficiency tables (Version 65). Prog. Photovolt. Res. Appl. 33, 3–15 (2025). https://doi.org/10.1002/pip.3867

[2] Wang, M., Wang, W., Ma, B., Shen, W., Liu, L., Cao, K., Chen, S., Huang, W.: Lead-free perovskite materials for solar cells. Nano-Micro Lett. 13, 62 (2021). https://doi.org/10.1007/s40820-020-00578-z

[3] Lei, H., Hardy, D., Gao, F.: Lead-free double perovskite Cs2AgBiBr6: Fundamentals, applications, and perspectives. Adv. Funct. Mater. 31, 2105898 (2021). https://doi.org/10.1002/adfm.202105898

[4] Tao, Q., Xu, P., Li, M., et al.: Machine learning for perovskite materials design and discovery. npj Comput. Mater. 7, 23 (2021). https://doi.org/10.1038/s41524-021-00495-8

[5] Im, J., Lee, S., Ko, T.W., et al.: Identifying Pb-free perovskites for solar cells by machine learning. npj Comput. Mater. 5, 37 (2019). https://doi.org/10.1038/s41524-019-0177-0

[6] Wu, C., Zhang, Q., Liu, Y., Luo, W., Guo, X., Huang, Z., Ting, H., Sun, W., Zhong, X., Wei, S., Wang, S., Chen, Z., Xiao, L.: The dawn of lead-free perovskite solar cell: Highly stable double perovskite Cs2AgBiBr6 film. Adv. Sci. 5, 1700759 (2018). https://doi.org/10.1002/advs.201700759

[7] Slavney, A.H., Hu, T., Lindenberg, A.M., Karunadasa, H.I.: A bismuth-halide double perovskite with long carrier recombination lifetime for photovoltaic applications. J. Am. Chem. Soc. 138, 2138–2141 (2016). https://doi.org/10.1021/jacs.5b13294

[8] Bartesaghi, D., Slavney, A.H., Gélvez-Rueda, M.C., et al.: Charge carrier dynamics in Cs2AgBiBr6 double perovskite. J. Phys. Chem. C 122, 4809–4816 (2018). https://doi.org/10.1021/acs.jpcc.8b00572

[9] Zhang, Z., Sun, Q., Lu, Y., Lu, F., Mu, X., Wei, S.-H., Sui, M.: Hydrogenated Cs2AgBiBr6 for significantly improved efficiency of lead-free inorganic double perovskite solar cell. Nat. Commun. 13, 3397 (2022). https://doi.org/10.1038/s41467-022-31016-w

[10] Xiao, B., et al.: Band matching strategy for all-inorganic Cs2AgBiBr6 double perovskite solar cells with high photovoltage. ACS Appl. Mater. Interfaces 13, 37027–37034 (2021). https://doi.org/10.1021/acsami.1c07169

[11] Raj, A., Kumar, M., Kumar, A., Laref, A., Anshul, A.: Investigating the potential of lead-free double perovskite Cs2AgBiBr6 material for solar cell applications: A theoretical study. Int. J. Energy Res. 46, 13801–13819 (2022). https://doi.org/10.1002/er.8099

[12] Uddin, M.S., Hossain, M.K., Uddin, M.B., Toki, G.F.I., Ouladsmane, M., Rubel, M.H.K., Tishkevich, D.I., Sasikumar, P., Haldhar, R., Pandey, R.: An in-depth investigation of the combined optoelectronic and photovoltaic properties of lead-free Cs2AgBiBr6 double perovskite solar cells using DFT and SCAPS-1D frameworks. Adv. Electron. Mater. 10, 2300751 (2024). https://doi.org/10.1002/aelm.202300751

[13] Yadav, S.C., Satrughna, J.A.K., Shirage, P.M.: Investigation of the potential solar cell application of Cs2AgBiBr6 lead-free double perovskite. J. Phys. Chem. Solids 181, 111515 (2023). https://doi.org/10.1016/j.jpcs.2023.111515

[14] Sabbah, H., Abdel Baki, Z., Mezher, R., Arayro, J.: SCAPS-1D modeling of hydrogenated lead-free Cs2AgBiBr6 double perovskite solar cells with a remarkable efficiency of 26.3%. Nanomaterials 14, 48 (2024). https://doi.org/10.3390/nano14010048

[15] Raj, A., Kumar, M., Singh, D.V., Singh, B., Dwivedi, D.K., Anshul, A.: Physical parameter optimization and band alignment approach for efficiency improvement in Cs2AgBiBr6 based lead-free perovskite solar cells. Sci. Rep. 15, 32868 (2025). https://doi.org/10.1038/s41598-025-02203-8

[16] Cui, W., Zhao, Y., Cui, C., et al.: Improved performance of double Cs2AgBiBr6 perovskite solar cells by engineering passivation defects with Co2+ additives. Vacuum 220, 112816 (2024). https://doi.org/10.1016/j.vacuum.2023.112816

[17] Bansal, N.K., Mishra, S., Dixit, H., Porwal, S., Singh, P., Singh, T.: Machine learning in perovskite solar cells: Recent developments and future perspectives. Energy Technol. 11, 2300735 (2023). https://doi.org/10.1002/ente.202300735

[18] Li, J., Pradhan, B., Gaur, S., Thomas, J.: Predictions and strategies learned from machine learning to develop high-performing perovskite solar cells. Adv. Energy Mater. 9, 1901891 (2019). https://doi.org/10.1002/aenm.201901891

[19] Zhan, H., Wang, M., Chen, J., Yin, X., Yue, Y., Lu, J.: Predicting photovoltaic parameters of perovskite solar cells using machine learning. J. Phys.: Condens. Matter 36, 355901 (2024). https://doi.org/10.1088/1361-648X/ad512d

[20] Li, W., Hu, J., Chen, Z., Jiang, H., Wu, J., Meng, X., Xu, F., Lin, J., Ma, X., Yang, T., Cheng, P., Xie, R.: Performance prediction and optimization of perovskite solar cells based on the Bayesian approach. Sol. Energy 262, 111853 (2023). https://doi.org/10.1016/j.solener.2023.111853

[21] Mammeri, M., Dehimi, L., Bencherif, H., Amami, M., Ezzine, S., Pandey, R., Hossain, M.K.: Targeting high performance of perovskite solar cells by combining electronic, manufacturing and environmental features in machine learning techniques. Heliyon 9, e21498 (2023). https://doi.org/10.1016/j.heliyon.2023.e21498

[22] Yusuf, A.S., Ramalan, A.M., Abubakar, A.A., Mohammed, I.K.: Effect of electron transport layers, interface defect density and working temperature on perovskite solar cells using SCAPS 1-D software. East Eur. J. Phys. 1, 332–341 (2024). https://doi.org/10.26565/2312-4334-2024-1-31

[23] Ram, H., Singh, R.S., Singh, A.K.: Simulations of the best thickness and temperature for perovskite CH3NH3SnI3-based solar cells with absorber layers. Russ. Phys. J. 68, 1998–2006 (2025). https://doi.org/10.1007/s11182-025-03645-3

[24] Nowsherwan, G.A.: Performance engineering of Cs2InSbCl6 lead-free double perovskite solar cells: Insights from DFT, SCAPS-1D, wxAMPS, AFORS-HET, Oghmanano, and COMSOL. Discov. Mater. 6, 15 (2026). https://doi.org/10.1007/s43939-025-00466-6

[25] Pandey, S., Shukla, N., Sharma, V.K., et al.: Machine learning-assisted first-principles investigation of structural, electronic, and photovoltaic properties of perovskite materials. Appl. Nanosci. 16, 53 (2026). https://doi.org/10.1007/s13204-026-03184-4

[26] Giannozzi, P., Baroni, S., Bonini, N., et al.: Quantum ESPRESSO: A modular and open-source software project for quantum simulations of materials. J. Phys.: Condens. Matter 21, 395502 (2009). https://doi.org/10.1088/0953-8984/21/39/395502

[27] Perdew, J.P., Burke, K., Ernzerhof, M.: Generalized gradient approximation made simple. Phys. Rev. Lett. 77, 3865–3868 (1996). https://doi.org/10.1103/PhysRevLett.77.3865

[28] Breiman, L.: Random forests. Mach. Learn. 45, 5–32 (2001). https://doi.org/10.1023/A:1010933404324

[29] Nishidate, K.: BURAI: GUI System for Quantum ESPRESSO. Iwate University, Morioka (2018).